Progress in Organic Coatings 99 (2016) 230–239

Contents lists available at ScienceDirect

Progress in Organic Coatings

journal homepage: www.elsevier.com/locate/porgcoat

Photocurable resin/microcrystalline cellulose composites for wood protection: Physical-mechanical characterization

Annalisa Cataldi[a], Carola Esposito Corcione[b], Mariaenrica Frigione[b], Alessandro Pegoretti[a,*]

[a] University of Trento, Department of Industrial Engineering and INSTM Unit Via Sommarive 9, Povo 38123, Trento, Italy
[b] University of Salento, Department of Innovation Engineering, Via Monteroni, 73100 Lecce Italy

ARTICLE INFO

Article history:
Received 26 February 2016
Received in revised form 11 May 2016
Accepted 26 May 2016

Keywords:
Photocuring
Microcrystalline cellulose
Composites
Mechanical properties
Protective coatings
Wood

ABSTRACT

Photocurable composites based on a UV-light curable methacrylic-siloxane resin formulation and various concentrations (5 ÷ 20 wt%) of microcrystalline cellulose powder (MCC) were prepared and characterized to assess their suitability as protective coatings for wooden artworks. Dynamic mechanical thermal analysis highlighted that MCC promoted an enhancement of both storage and loss moduli and a decrease of the thermal expansion coefficient. Interestingly, the flexure elastic modulus and the flexure maximum stress of the neat photoresin increased upon the filler addition without any embrittling effect. An increment of hydrophobicity (contact angle), surface hardness (Shore D and pencil scratch tests) of the neat UV-light cured matrix even at the lowest filler loading was observed. These promising results suggest that the photo-curable microcomposites could be able to recover the mechanical and physical properties of damaged wood and replace the traditional resins soluble in toxic solvents utilized in this kind of restoration works.

1. Introduction

Wood is one of the most common constituent materials of cultural heritage. It was one of the first materials utilized for building. Wood was widely used in the past for outdoor and indoor purposes, to make artworks such as eating utensils, decorations of buildings and churches or egg-based paintings. This material is very sensitive to decay and several degradative processes can attack it [1].

Chemical, physical, biological or mechanical decay leads to similar effects on wood, in particular promotes the reduction of its mechanical strength [2,3]. In order to recover wooden artworks subjected to a critical degradation state, conservators choose to protect and consolidate objects by the application of a liquid synthetic resin through brush, spray, injection or the direct immersion [4,5]. In particular, Paraloid B72 is certainly one of the most utilized protective materials for damaged wood because it guarantees good performances [6]. A typical wood restoration treatment with Paraloid B72 consists of the application by brush of solutions at 3–10 wt% of this acrylate in acetone or even stronger and toxic solvents. A possible and promising solution to this drawback could be the application of curable monomers/oligomers, that, having a lower viscosity with respect to polymers, do not require the use of solvents. Recently, Cataldi et al. have successfully produced microcomposites consisting of Paraloid B72 filled with MCC. The Paraloid/MCC composites were characterized and tested as protective materials for hystorical damaged wood samples with positive results [7,8]. In fact, cellulose based fillers are more and more utilized in the wood protection [9,10]. In particular, MCC was selected for its well-known reinforcing properties [11,12] and its chemical affinity with wood having the same chemical composition. Moreover, MCC is easy to source, conservators can handily use it because it does not require any other chemical process to be applied.

Corcione et al. have characterized curable formulations based on siloxane and methacrylic or acrylic monomers in terms of adhesion on surfaces, hydrophobicity, optical transparency, capability to prevent infiltration of contaminants or degrading agents, permeability to water vapor, chemical compatibility with different inorganic substrates, finding excellent antifouling and weathering resistance [13,14]. The low molecular weight of the monomers, the low viscosity of the formulation, as well as the in situ polymerization mechanism, allow the resin penetration inside porous substrates, such as stones or wood, leading to a uniform and very adherent hydrophobic coating [13]. Such properties make them optimal materials for manufacturing water repellent and optically

* Corresponding author.
E-mail addresses: annalisa.cataldi@unitn.it (A. Cataldi), alessandro.pegoretti@unitn.it (A. Pegoretti).

http://dx.doi.org/10.1016/j.porgcoat.2016.05.015
0300-9440/

clear coatings for protection and conservation of wood, stones and concrete buildings, lens, dental elements and adhesives and multifunctional finishing agents for textiles and leather components [15]. Guo et al. have utilized a UV-light photoinitiator for activating photopolymerization of formulations based on such monomers as a valuable alternative to the thermally initiated curing [16], that is an approach typically used for preparing coatings for protection of natural stones or wood artworks. UV-light photoinitiation is a solvent-free curing mechanism based on a photopolymerization faster than that activated by a thermal initiator [15]. Indeed, thermal curing requires up to several weeks to complete the reaction, and, hence, it is strongly affected by environmental conditions (i.e. temperature, humidity and external contamination). The fast UV curing process results, especially in outdoor and large surface area applications, in highly adherent, stable and, completely cured coatings, exhibiting a glass transition temperature (Tg) higher than those achieved by means of thermal polymerization or by solution processes, whose Tg anyway never exceeds 40 °C.

In the present work the introduction of microcrystalline cellulose into a UV-light curable methacrylic-siloxane resin formulation (photoresin) is considered for a potential improvement of its performances as protective coating for wood. The photoresin, recently optimized by the authors, is based on both methacrylic and siloxane monomers, namely trimethylolpropane trimethacrylate (TMPTMA), (trimethoxysilyl)propylmethacrylate (MEMO) and a vinyl terminated polydimethylsiloxane (VT PDMS), that are UV-light photoinitiated by Irgacure819. This work represents the preliminary characterization of photocurable composites filled with microcrystalline cellulose, in view of the application of these materials as protective coatings on degraded wood.

2. Experimental

2.1. Materials

Trimethylolpropane trimethacrylate (TMPTMA) was chosen as the main component for the coating due to its high reactivity. The product used was supplied by Cray Valley.

A trimethoxypropyl silane methacrylate monomer, produced by Dow Corning as Z6030 and known as MEMO, was used as a coupling agent.

A vinyl terminated polydimethylsiloxane (VT PDMS), supplied by Aldrich, was added to the methacrylic mixture to enhance the coatings' water resistance.

A 3-mercaptopropyltriethoxysilane (MPTS), supplied by Aldrich, was added to the siloxane modified methacrylic resin system in order to reduce the effect of inhibition of oxygen towards radical photopolymerization. MPTS has an average molecular weight of about 238.42 g/mol.

The functionalization of VT PDMS with MPTS was done by mixing the two components at 100 °C in 1:1 molar ratio in presence of 1% wt. of diethylamine (DTA), again supplied by Aldrich. The chemical formula of all components are reported in Fig. 1.

Bis(2,4,6-trimethylbenzoyl)-phenylphosphineoxide, supplied by Ciba as IRGACURE 819, was added to the polymeric formulation in a content of 1 pph to activate the photopolymerization reaction upon UV exposure.

Microcrystalline cellulose powder (MCC) (Sigma Aldrich, USA) with a specific gravity of 1.56g cm^{-3} and a mean molecular weight of 90.000 g/mol was selected as a filler.

2.2. Preparation of UV-curable microcomposites

Composites with a MCC amount from 5 wt% to 20 wt% were prepared through the mechanical mixing of the photoresin with the microfiller under magnetic stirring at room temperature. All formulations were poured in the cavities of silicon molds and introduced into a UV-chamber equipped with six UVB lamps model UVB 313EL (Q-lab corporation, UK) with a maximum peak of emission centered at 315 nm and a total power of 480 W. A curing cycle of 24 h was conducted. Samples for mechanical tests were conditioned at 23 °C and 55% of relative humidity in a chamber with a super saturated solution of $Mg(NO_3)_2{\cdot}6H_2O$ until the reaching of the equilibrium conditions. This is the indoor humidity level recommended for the optimal artwork conservation and fruition [17]. Composites samples were denoted indicating the photomatrix, the filler (MCC) and its weight concentration. The compositions of the experimental formulations produced is outlined in Table 1.

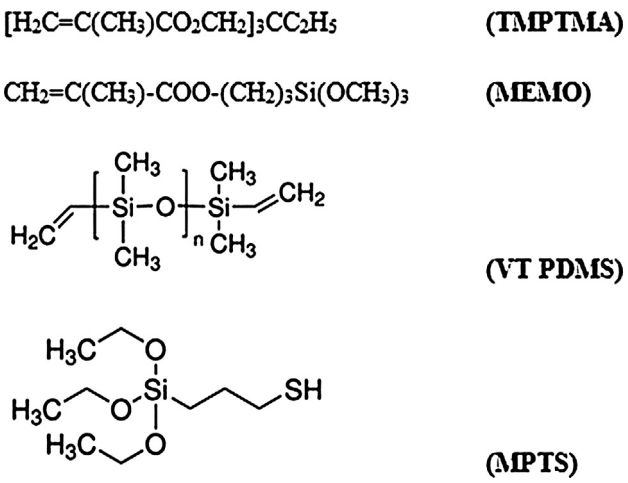

Fig. 1. Chemical formula of the photomatrix constituents.

Table 1
Composition of the experimental formulations produced.

System	Weight percentage (% wt.)
photomatrix	85% TMPTMA 4.97% VTPDMS 0.03% MPTS 10% MEMO
photomatrix-MCC-5	95% photomatrix 5% MCC
photomatrix-MCC-10	90% photomatrix 10% MCC
photomatrix-MCC-20	80% photomatrix 20% MCC

2.3. FESEM analysis

Microstructural observations on cryofractured surfaces of the neat photomatrix and the corresponding microcomposites samples were carried out by a Zeiss Supra 40 high resolution FESEM microscope with an accelerating voltage of 1.5 kV and a beam aperture of 20 μm.

2.4. Rheological tests

The rheological characterization of each liquid formulation was carried out in a strain controlled Rheometer (Ares Rheometric Scientific). The tests were performed with a plate/plate geometry (radius = 12.5 mm) under steady state mode, at room temperature (25 °C) using a shear rate ranging from 0.05 to 100 s^{-1}. A first sweep experiment was always followed by a second one performed

on the same sample and using the same conditions, in order to avoid any aggregation of the filler. The rheological experiments were repeated at least three times to check the repeatability of results.

2.5. Thermal analysis

Differential scanning calorimetry (DSC) measurements were performed by using a Mettler Toledo TC15 calorimeter. Samples of about 10 mg were analyzed under a nitrogen flow of 150 ml min^{-1}, applying a first heating stage from 0 to 250 °C linked to a cooling stage from 250 to 0 °C, and to a second heating stage until 250 °C at 10 °C min^{-1}. The glass transition temperature (Tg) was evaluated as the inflection point in the thermograms of the first heating stage. In the second heating scan it was not possible to observe the Tg signal as an inflection point. The determination of the glass transition temperature of all samples in the second heating stage, was carried out through the derivative of the specific power in the range of temperature 0–100 °C and the fitting of the peak corresponding to the T_g signal. At least three specimens for each formulation were analyzed and the calorimetric results averaged.

Thermal stability of the photocured composites was investigated through thermogravimetric analysis (TGA), by using a Mettler TG50 thermobalance in a temperature interval between 25 and 700 °C, at a heating rate of 10 °C min^{-1}, and under a nitrogen flow of 150 ml min^{-1}. The onset temperature (i.e., the temperature associated to a mass loss of 5%) and the residual mass at 700 °C were determined. The maximum degradation temperature was evaluated from the peak of mass loss rate curve. At least three specimens were tested for each composition.

2.6. DMTA analysis

Dynamic mechanical thermal analysis (DMTA) were performed by a TA Instruments DMA Q800 device under tensile configuration on at least three rectangular specimens 15 mm long, 5 mm wide and 0.25 mm thick. The thermograms of the storage modulus (E′), loss modulus (E″) and loss tangent (tanδ) were measured in a temperature range between −10 °C and 120 °C, at a heating rate of 3 °C min^{-1} and a frequency of 1 Hz. The strain amplitude was fixed at 0.05%, in order to assure a linear viscoelastic behavior. From the slope of the thermal strain curves it was possible to determine the coefficients of linear thermal expansion (CLTE) below Tg (i.e. in a temperature interval between 0 °C and 40 °C) and above Tg (between 70 °C and 100 °C).

2.7. Three-points bending tests

According to ASTM D790 standard three-points bending tests were carried out on samples consisting of at least 5 rectangular specimens (width = 5 mm, thickness = 2.5 mm, span length = 40 mm) for each set of samples by means of an Instron 4502 universal testing machine, equipped with a 1 kn load cell. A crosshead speed of 1 mm/min was used. In this way it was possible to evaluate the flexural modulus (E_f), the maximum flexural stress ($\sigma_{MAX,f}$) and the maximum flexural strain ($\varepsilon_{MAX,f}$) of examined specimens.

2.8. Hardness tests

Hardness Shore D measurements on the photocured samples (rectangular specimens width = 5 mm, thickness = 2.5 mm, span length = 40 mm) was performed by a digital durometer Sh D, Gibitre Instruments, according to ASTM D2240. Five tests were performed for each sample.

The scratch hardness of the photocured films (about 100 μm thickness) was finally measured with Pencil hardness test, according to Standard Test Method for Film Hardness by Pencil Test, ASTM D 3633.

2.9. Static contact angle measurements

Static contact angle measurements were performed with a COSTECH instrument, equipped with a videocamera. The analyses were performed at room temperature by means of the sessile drop technique, according to NORMAL Protocol 33/89. Thirty measurements were performed on each sample (rectangular specimen 25 mm long, 5 mm wide and 2.5 mm thick) and the results were averaged. The measuring liquid was bi-distilled water (surface tension γ = 72.1 mN/m).

2.10. Water sorption tests

The moisture content, M%, was determined by monitoring the change of weight of at least five specimens for each formulation, by using a Gibertini E42 electronic balance with an accuracy of 10^{-4} g. According to ASTM D570 standard, M% was calculated by the comparison between the initial weight of the samples (W_0) and the weight at the equilibrium point (W_t) according to Eq. (1):

$$M\% = 100\frac{(W_t - W_0)}{W_0} \quad (1)$$

where W_t is the wet weight of specimens at the equilibrium point and W_0 is the initial dry weight of specimens. Moreover, according to ASTM D5229 standard, the final moisture content (Mmax) and the time required to reach the equilibrium water content (ts) were evaluated.

3. Results and discussion

3.1. Microstructure analysis

MCC particles consist of elongated flakes with an average length (L) of about 24 μm and a diameter (D) of about 10 μm (average L/D ratio of 2.4). ESEM image of MCCs used in this work is reported in the ref. [18].

In order to evaluate the dispersion degree of MCC within the matrix, FESEM observations of cryofractured surfaces of the neat matrix and the corresponding composites were carried out. FESEM images of neat matrix and composites filled with 5–10 and 20 wt% of MCC are showed in Fig. 2(a–d). All filled samples present microcellulose particles uniformly dispersed in the photoresin without any preferential orientation and any significant agglomeration phenomena.

3.2. Rheological behavior of composites

The viscosity of unfilled photocurable resin measured in a plate and plate rheometer in two subsequent sweep experiments is plotted as a function of the shear rate in Fig. 3. In the same figure, the flow curves of the photomatrix filled with 5 wt%, 10 wt% and 20 wt% of MCC particles are also displayed. Each formulation displays a moderate pseudo-plastic behavior, with no appreciable differences between the two subsequent rheological measurements, which indicates the absence of any possible effect of aggregation of the MCC filler. However, a pre-shear step was always performed on the mixtures before every rheological measurement. The rheological curves shown in Fig. 3 display the typical behavior of filled resins. The viscosity increases with increasing the weight fraction of MCC, assuming a value almost independent from the shear rate at higher values. It is worthwhile to underline that the viscosity of the

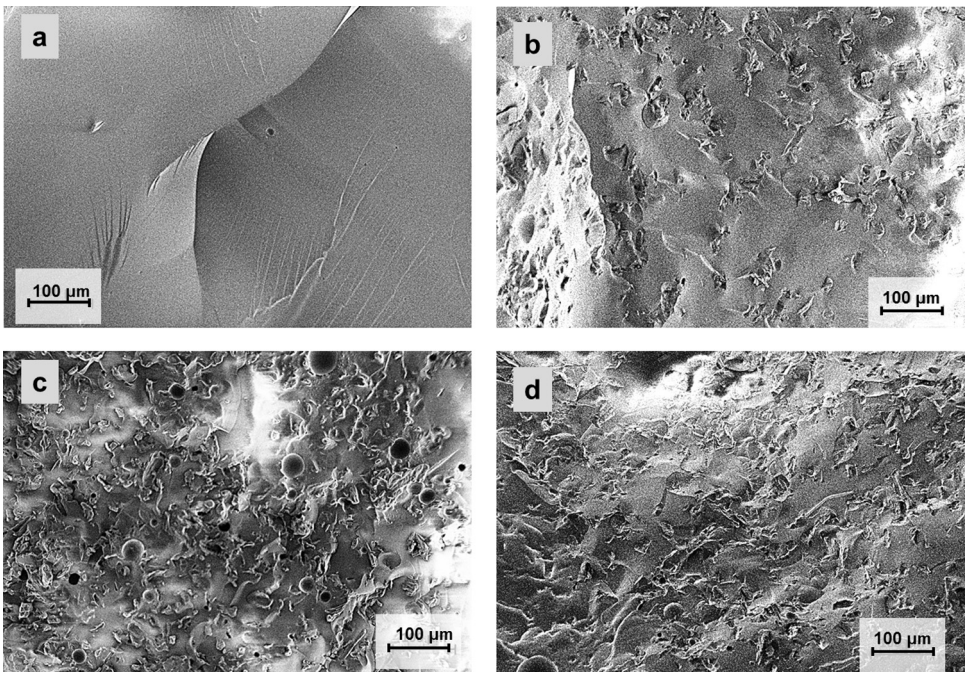

Fig. 2. FESEM images of the cryofractured surfaces of neat photoresin and corresponding microcomposites. (a) Photomatrix, (b) photomatrix-MCC-5, (c) photomatrix-MCC-10, (d) photomatrix-MCC-20.

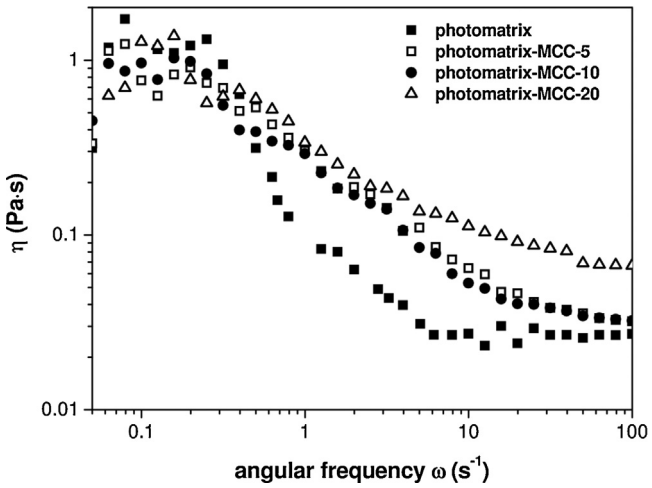

Fig. 3. Apparent viscosity of neat photomatrix and its corresponding microcomposites.

investigated polymer remains suitable for the specific application even at the highest MCC content. The most common commercial and experimental available products are, in fact, applied by brushing and a viscosity of about 0.1-0.3 Pa*s at shear rate of 10 s^{-1} has been always considered suitable for the application of the coating on wood [13]. A similar behavior was already reported for liquid mixtures containing nano-fillers, such as montmorillonite, and attributed to the shape of the nano-filler exhibiting a certain amount of orientation with increasing the shear rate [19]. The rheological behavior of each formulation was also monitored as a function of storing time, i.e., at five and six months from their preparation. The viscosity curves obtained for each systems were always equal to those reported in Fig. 3, evidencing the stability of the formulations, even after six months from their production. This result is an indirect evidence of the capability of the preparation method used to produce a stable and well dispersed organic-inorganic composite system, with no separation phase.

3.3. Thermal analysis

Fig. 4 (a-b) represents DSC thermograms of neat photomatrix and relative composites collected during first and second heating stage. All specimens show the typical trend of amorphous polymers, with the presence of an inflection point at around 57 °C in the thermograms visible in the first heating stage due to the glass transition temperature. In the second scan, since it was not possible to observe the T_g signal as an inflection point, the glass transition temperature of all samples was evaluated by the fitting of the peak resulting from the derivative of the specific power in the temperatures interval 0–100 °C. In Table 2 the main results from DSC analysis are summarized. As one can notice, there is no significant effect due to MCC introduction on the glass transition temperature of the pure matrix, just a slight increase of this property after the filler addition is evident in the first stage. Samples at 5 wt% of microfiller present a value of the curing residual heat ($\Delta H_{residual}$), normalized with respect to the actual resin content, similar to that of the matrix. While, formulations with a MCC loading higher than 5 wt% exhibit a higher $\Delta H_{residual}$ in comparison to the unfilled photoresin and a consequent decrease of the T_g in the second heating stage. This could be explain through a reduction/inhibition of the photocurable resin reactivity produced by high contents of MCC related to the scattering of light from MCC particles. The scattering from particles acts like a shield preventing light penetration in the underlying suspension. It has been found empirically that the scattering yield depends on the particle size, on the ratio of the inter-particle spacing to the radiation wavelength and on the square of the refractive index difference between the different phases [20]. Nevertheless the reactivity of the suspension with the highest content of MCC particles is still suitable for the specific application [13].

Thermal resistance properties of the constituents and the relative composites are listed in Table 3. TGA thermograms of all materials are reported in Fig. 5a, while in Fig. 5b the derivative of the mass loss curves is represented. MCC introduction does not affect the thermal stability of the pure resin even at highest filler loadings. However, filled samples register a progressive decrease of the

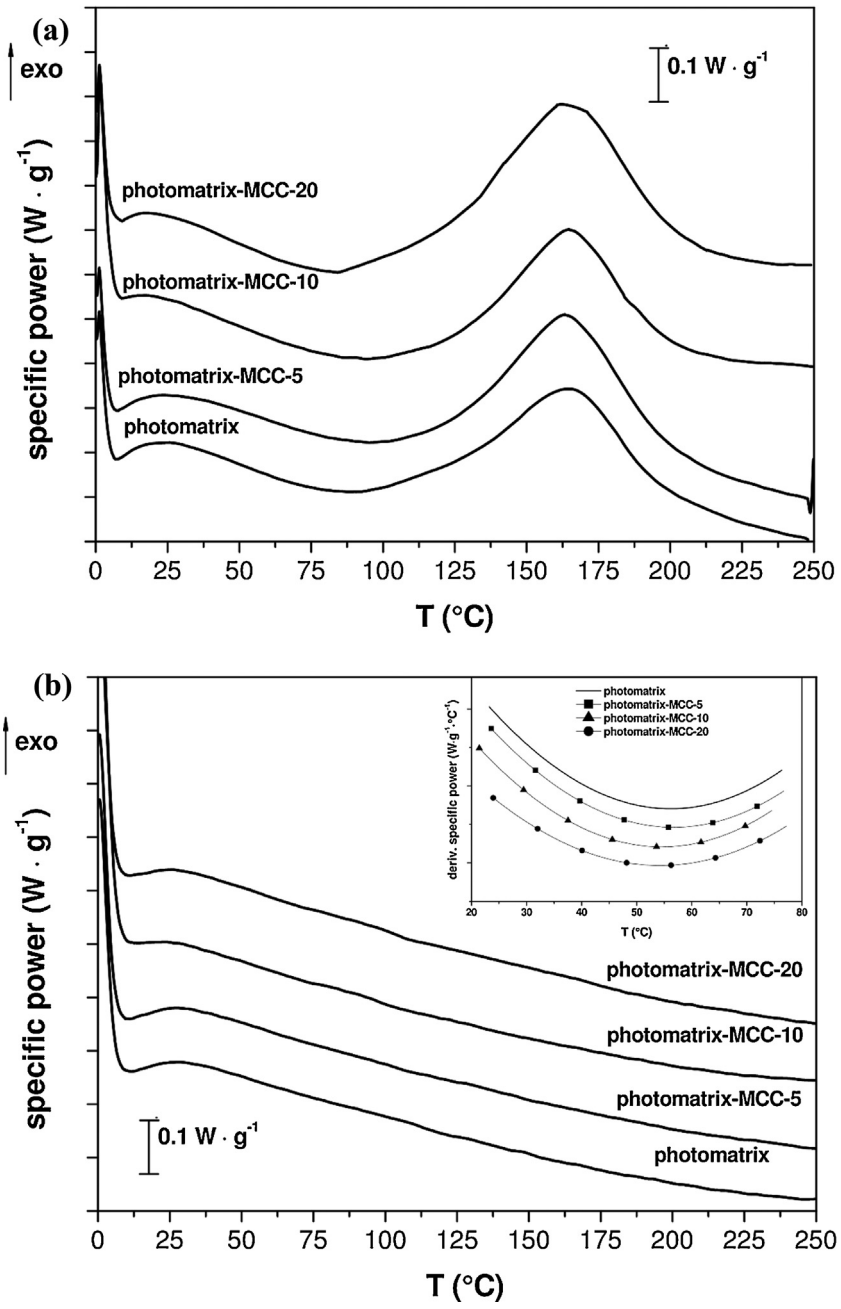

Fig. 4. DSC thermograms of neat photoresin and corresponding microcomposites. (a) First heating stage, (b) second heating stage.

Table 2
Glass transition temperature (T_g) and curing residual heat ($\Delta H_{residual}$) of neat photoresin and corresponding microcomposites.

Tg (°C)			$\Delta H_{residual}$ (J g^{-1})
Sample	I scan Inflection point	II scan Peak derivative curve	
photomatrix	56.6 ± 1.2	59.0 ± 0.6	51.8 ± 0.2
photomatrix-MCC-5	58.9 ± 0.8	59.2 ± 0.6	53.3 ± 0.4
photomatrix-MCC-10	57.1 ± 1.0	57.6 ± 0.4	57.8 ± 0.7
photomatrix-MCC-20	57.9 ± 0.5	57.0 ± 0.2	69.5 ± 0.4

$\Delta H_{residual}$: Residual heat of the cure reaction normalized with respect to the resin content.

onset temperature as the filler content increases due to the lower thermal stability of microcellulose with respect to the photomatrix. From Fig. 5b one can notice the presence of two degradation peaks at around 270 °C and 470 °C in all filled composites curves. The early degradation stage is more evident for formulations with 20 wt% of MCC. This degradation peak was detected in other studies on MCC polymer composites [21], it may be related to a small fraction of MCC particles that starts to degrade before the matrix. The residual mass at 700 °C increases proportionally to the filler content maybe because of the formation of a char layer on the surface

Table 3
Results of TGA test on neat photoresin and corresponding microcomposites.

Sample	T_{onset} (°C)	T_{MAX} (°C)	Residual mass at 700 °C (%)
photomatrix	366	472	3.4
photomatrix-MCC-5	305	472	4.0
photomatrix-MCC-10	298	472	6.6
photomatrix-MCC-20	275	472	7.5
MCC	291	337	0.8

Tonset = temperature of the initial degradation step (corresponding to a mass loss of 5 wt%).
T_{MAX} = temperature of the maximum degradation rate.

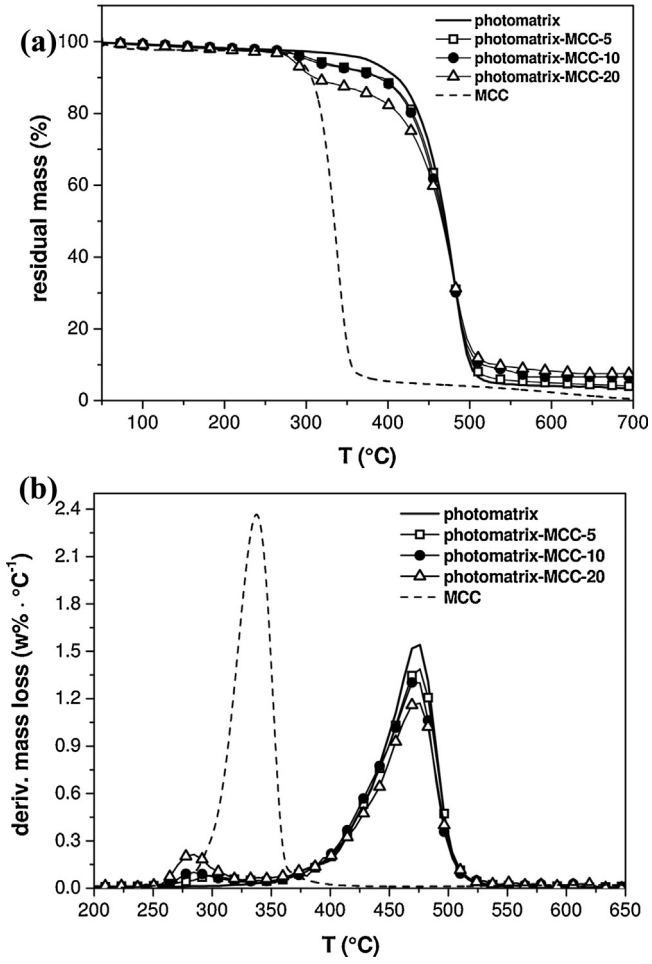

Fig. 5. TGA thermograms of neat photoresin, neat MCC, and corresponding microcomposites. (a) Residual mass as a function of temperature, (b) derivative of the mass loss.

of the samples, which does not allow the complete combustion and vaporization of the matrix.

3.4. Dynamic mechanical thermal analysis and thermal expansion

The effect of MCC on the viscoelastic properties of the photomatrix was investigated by DMTA analysis. In Fig. 6(a–b) the trends of relative storage modulus (E′ at 25 °C) and loss modulus (E″) peak calculated as the ratios between the composites values and the neat matrix values are reported, while, in Table 4 the most relevant data obtained from DMTA analysis are summarized. MCC is able to promote an increment of both storage and loss moduli. The consequent decrease of tanδ that is the ratio between E″ and E′ suggests a more pronounced contribution of cellulose microcrys-

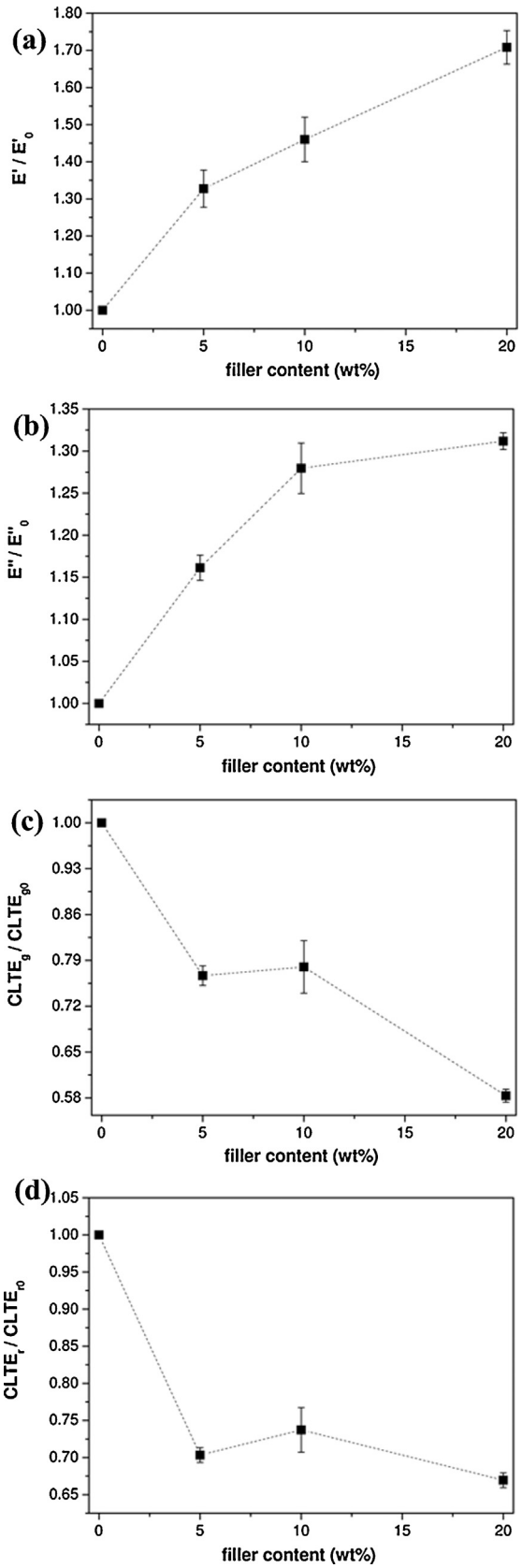

Fig. 6. Main results from DMTA analysis: (a) relative storage modulus, E′, (b) relative loss modulus, E″, (c) relative coefficient of linear thermal expansion below T_g, $CLTE_g$, (d) relative coefficient of thermal expansion linear above T_g, $CLTE_r$.

Table 4
Results of DMTA tests on neat photoresin and corresponding microcomposites.

Sample	E' (GPa) at 25 °C	E" (GPa) peak value	tanδ peak value	Tg (°C) from tanδ	CLTEg (K^{-1})	CLTEr (K^{-1})
photomatrix	1.13 ± 0.12	0.093 ± 0.012	0.074 ± 0.008	71.7 ± 0.9	6.07E-05 ± 2.43E-07	1.18E-04 ± 6.16E-08
photomatrix-MCC-5	1.50 ± 0.14	0.108 ± 0.003	0.069 ± 0.005	74.0 ± 0.8	4.63E-05± 1.87E-07	0.83E-04 ± 2.18E-08
photomatrix-MCC-10	1.65 ± 0.11	0.119 ± 0.008	0.053 ± 0.005	67.1 ± 0.3	4.90E-05 ± 1.63E-07	0.87E-04 ± 8.06E-08
photomatrix-MCC-20	1.93 ± 0.15	0.122 ± 0.002	0.045 ± 0.008	66.2 ± 0.6	3.55E-05 ± 1.08E-07	0.79E-04 ± 2.67E-08

E': storage modulus.
E": loss modulus.
tanδ: loss factor.
T_g: glass transition temperature.
$CLTE_g$: coefficient of linear thermal expansion in the glassy state (interval 0–40 °C).
$CLTE_r$: coefficient of linear thermal expansion in the rubbery state (interval 70–100 °C).

Table 5
Results of 3-points bending tests on neat photoresin and corresponding microcomposites.

Sample	E_f (GPa)	$\sigma_{MAX,f}$ (MPa)	$\varepsilon_{MAX,f}$
photomatrix	1.49 ± 0.04	22.19 ± 1.85	0.052 ± 0.002
photomatrix-MCC-5	1.98 ± 0.05	24.08 ± 1.18	0.046 ± 0.003
photomatrix-MCC-10	2.32 ± 0.05	26.75 ± 1.74	0.042 ± 0.001
photomatrix-MCC-20	2.46 ± 0.02	24.75 ± 0.91	0.043 ± 0.003

E_f: flexural modulus.
$\sigma_{MAX,f}$: maximum flexural stress.
$\varepsilon_{MAX,f}$: maximum flexural strain.

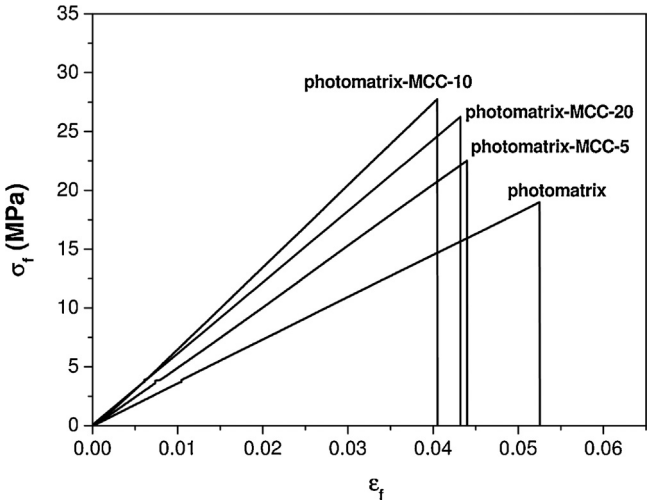

Fig. 7. Representative stress/strain curves of neat photomatrix and corresponding microcomposites from three points flexure tests.

tals on the matrix elastic components rather than on its dissipative ones. The systematic increases of E′ and E″ are proportional to the filler content. In particular, if filled samples can reach E″ values 30% higher than the neat photoresin, for E' there is an increment even until 70% in comparison to the unfilled matrix. Paraloid/MCC composites reported a similar viscoelastic response but, interestingly, the increase of E' was much lower than that observed for MCC filled photocured composites [8,18]. From the position of the E″ peak it is possible to assess the glass transition temperature of each composite sample. Even if it is hard to find a trend, formulations with 5 wt% of MCC register an increase of T_g of about 3°, but higher filler amounts lead to a decrease of this property (Table 4), as previously seen in the DSC results. A positive response exhibited by photocured systems after the addition of cellulose microcrystals is the progressive decrease of the linear thermal expansion coefficient below ($CLTE_g$) and above ($CLTE_r$) the glass transition temperature as the filler content increases. This is the typical stabilizing action played by microcellulose in improving the dimensional stability of polymeric matrices [21–23]. From Fig. 6(c–d) one can notice a remarkable reduction of CLTE in both glassy and rubbery states with values even 40% lower than the neat matrix. Also in this case, MCC is more effective into the photoresin than within Paraloid B72 for which a CLTE reduction up to 25% was reported [8,18].

3.5. Mechanical properties

Three points bending tests results confirm the stabilization of the photoresin due to MCC with an increase of the stiffening with increasing of the MCC content without any embrittling effect on the matrix. In Table 5 and in Fig. 7, reporting the most important flexural properties and the representative stress/strain curves of the neat photoresin and its corresponding microcomposites respectively, it is possible to observe a proportional enhancement of the flexural elastic modulus (E_f) and a slight increase of the maximum flexural stress ($\sigma_{MAX,f}$) with the filler loading. A slight decrease of the maximum flexural strain ($\varepsilon_{MAX,f}$) with the filler loading is observed as well. Fig. 8(a–b) shows the relative trends of E_f and $\sigma_{MAX,f}$ normalized over the corresponding properties of the neat matrix and highlights an increment up to around 70% of the stiffness and up to around 20% of the strength after the introduction of microcellulose. Interestingly, the improved elastic modulus of Paraloid/MCC composites was useful during the consolidation of damaged wood leading to an increment of the stiffness of this material where the pure paraloid was ineffective [7].

Shore D, pencil hardness and water contact angle of both unfilled and filled photocured systems were also measured and reported in Table 6. The Shore D surface hardness of the photocured systems confirms that the presence of the MCC particles appreciably enhances also the surface rigidity. In fact, by adding a small amount of MCC particles (10 wt%), a 12% increment of surface hardness of the coating was registered. Also, the scratch hardness of the photocured films increases due to MCC addition. In particular, the highest value (9H) was obtained with system, containing 5 wt% of MCC confirming the capability of the filler to improve the final properties of the polymeric matrix, even at the lowest percentage. These latter hardness results, along with the increase in the hydrophobicity of the MCC-filled systems, are particularly interesting for the specific applications where good surface mechanical properties and hydrophobicity are mandatory.

3.6. Contact angle and moisture uptake

As reported in Table 6, each system show a good hydrophobic behavior, evidenced by a contact angle much higher than 90° (Fig. 9). The neat photomatrix is already hydrophobic, exhibiting a contact angle of about 104°. The presence of MCC allowed the enhancement of this value up to 108°, irrespective of the amount of the filler. This result is very promising and suggests a possible use of the composites to protect and consolidate wood substrates by preventing the ingress of liquid water.

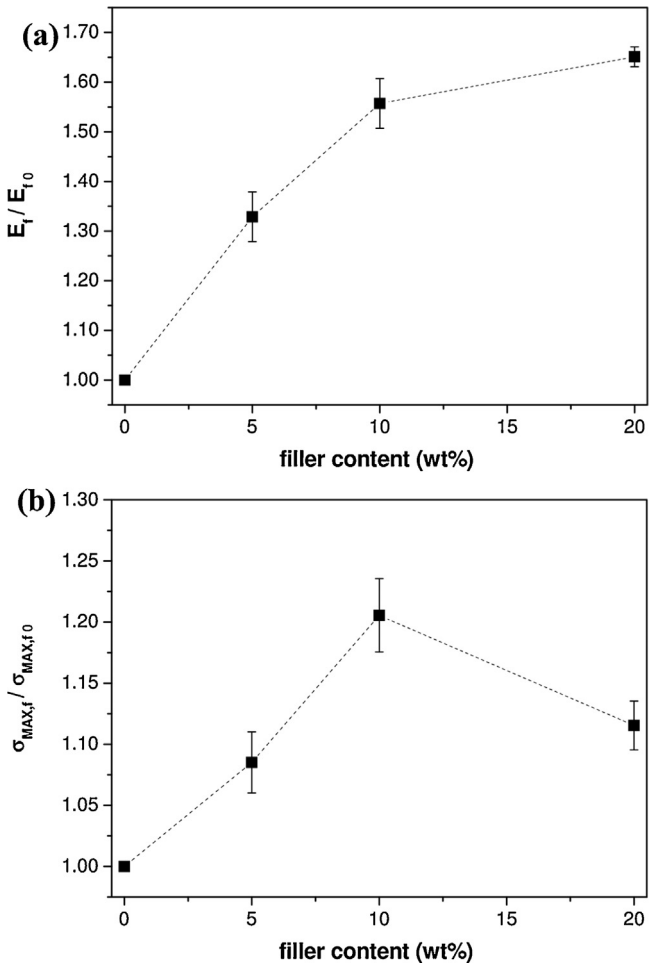

Fig. 8. Main relative flexure properties trends of neat photomatrix and corresponding microomposites. (a) flexural modulus, E_f, (b) maximum flexural stress, $\sigma_{MAX,f}$.

Table 6
Results of Shore D and pencil hardness tests, contact angle analysis, and water sorption tests on neat photoresin and corresponding microcomposites.

Sample	ShoreD	Pencil hardness	Contact angle (°)	M_{MAX} (wt%)	t_s (h)
photomatrix	81.0 ± 1.6	6H	103.5 ± 0.8	0.87	198
photomatrix-MCC-5	87.1 ± 0.2	>9H	107.7 ± 0.7	0.92	198
photomatrix MCC-10	92.9 ± 0.3	7H	107.7 ± 0.8	1.10	198
photomatrix-MCC-20	88.6 ± 0.5	7H	108.2 ± 0.3	1.25	198

M_{MAX}: Maximum moisture content at the equilibrium point.
ts: Time to reach the equilibrium point.

Thanks to water sorption tests it was possible to evaluate the moisture uptake kinetics (M%) of unfilled and filled matrix (Fig. 10). The maximum moisture content (M_{MAX}) and the time taken to reach the equilibrium conditions (t_s) are summarized in Table 6. Gravimetric curves of all formulations show a typical Fickian behavior, with an initial step exhibits a linear relationship between the humidity sorption and the square root of the time, typical of a Fickian diffusion. After this step, the water sorption rate decreases until an equilibrium point [24]. MCC powder sorbs less water than the neat resin. Despite this, the introduction of this microfiller leads to an increase of the moisture content in all composites samples proportionally to the MCC content. For instance, if M% of the pure photoresin is 0.87 wt%, samples with 20 wt% of MCC show an equilibrium moisture value of 1.25 wt%. Anyway the moisture increment is less than 0.5 wt% even after the addition of the highest MCC loading. A possible cause of this phenomenon could be related to the moisture absorption mechanism through microcraks, voids and other defects, including the filler-matrix interface [25,26]. In the FESEM images the presence of voids was not detected (Fig. 2). On the other hand, it is not possible through FESEM micrographs to evaluate in detail the filler-matrix interface. The higher tendency of filled photomatrix to absorb water after the introduction of MCC may be due to this capillary flow through the filler-matrix interface as already observed for Paraloid based microcomposites [8]. The time required to reach equilibrium conditions does not change upon the MCC introduction.

4. Conclusions

Various amounts of microcrystalline cellulose were added to a UV-light curable methacrylic-siloxane resin. Although MCC flakes produced a progressive increase of the filled composites viscosity, this property remains suitable for the restoration operations. The glass transition temperature and the thermal stability of the neat photoresin were not affected by the microcellulose presence. MCC addition produced an interesting stabilizing effect on the mechan-

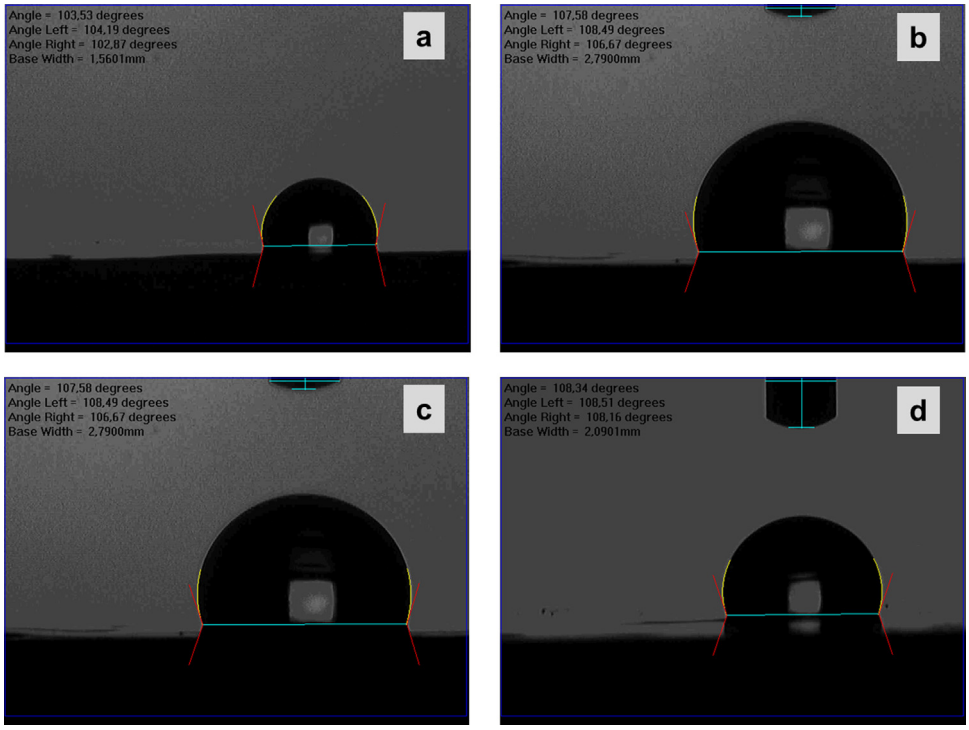

Fig. 9. Static contact angle of water on neat photomatrix and corresponding microcomposites.

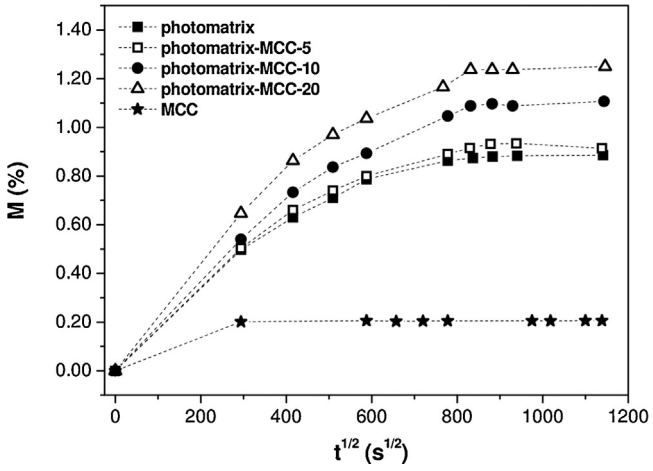

Fig. 10. Water uptake of MCC powder, neat photoresin and corresponding microcomposites conditioned at RH = 55% and T = 23 °C.

ical properties of the photoresin, with an increase of the dynamic moduli (E′, E″) and a systematic decrease of the thermal expansion coefficient, proportional to the filler content. Moreover, MCC introduction determined an increase of the flexure stiffness associated to an enhancement of the flexure strength. The increase of the hydrophobicity, Shore D and pencil hardness upon MCC addition into the neat UV-light cured matrix since the lowest filler loading was detected.

These results are a promising starting point for a following study on the application of these photocurable microcomposites as innovative protective coatings of damaged wood.

Conflict of interest

The Authors declare that there is no conflict of interest.

Acknowledgments

The support of Mr Lorenzo Moschini in the FESEM analysis is kindly acknowledged.

References

[1] A. Unger, A.P. Schniewind, W. Unger, Conservation of Wood Artifacts: A Handbook, Springer, 2001, 2016, pp. 578.
[2] L. Toniolo, A. Paradisi, S. Goidanich, G. Pennati, Mechanical behaviour of lime based mortars after surface consolidation, Constr. Build. Mater. 25 (2011) 1553–1559.
[3] G. Borsoi, M. Tavares, R.V. António Santos Silva, Studies of the Performance of Nanostructured and other Compatible Consolidation Products for Historical Renders. Mater Sci Forum. Ana Maria Pires Pinto and António Sérgio Pouzada (2012) 942–947.
[4] Y. Wang, A.P. Schniewind, Consolidation of deteriorated wood with soluble resins, J. Am. Inst. Conserv. 24 (1985) 77–91.
[5] V. Horie, Materials for Conservation: Organic Consolidants Adhesives and Coatings, Routledge, 2010.
[6] G.M. Crisci, M.F. La Russa, M. Malagodi, S.A. Ruffolo, Consolidating properties of Regalrez 1126 and Paraloid B72 applied to wood, J. Cult. Heritage 11 (2010) 304–308.
[7] A. Cataldi, F. Deflorian, A. Pegoretti, Microcrystalline cellulose filled composites for wooden artwork consolidation: application and physic-mechanical characterization, Mater. Des. 83 (2015) 611–619.
[8] A. Cataldi, A. Dorigato, F. Deflorian, A. Pegoretti, Effect of the water absorption on the mechanical behaviour of microcrystalline cellulose filled composites for art protection and restoration, J. Appl. Polym. Sci. 131 (2014) 9070–9075.
[9] M. Christensen, H. Kutzke, F.K. Hansen, New materials used for the consolidation of archaeological wood–past attempts, present struggles, and future requirements, J. Cult. Heritage 13 (2012) S183–S190.
[10] A.A. Tuduce-Trăistaru, M. Câmpean, M.C. Timar, Compatibility indicators in developing consolidation materials with nanoparticle insertions for old wooden objects, Int. J. Conserv. Sci. 1 (2010) 219–226.
[11] P. Thummanukitcharoen, S. Limpanart, K. Srikulkit, Preparation of organosilane treated microcrystalline cellulose (Simcc) and the Polypropylene/Simcc composite, in: 18th International Conference On Composite Materials, Jeju Island, Korea, 2011.
[12] S. Spoljaric, A. Genovese, R.A. Shanks, Polypropylene–microcrystalline cellulose composites with enhanced compatibility and properties, Composites Part A 40 (2009) 791–799.
[13] C.E. Corcione, M. Frigione, UV-cured polymer-boehmite nanocomposite as protective coating for wood elements, Prog. Org. Coat. 74 (2012) 781–787.

[14] C. Ingrosso, C. Esposito Corcione, R. Striani, et al., UV-Curable nanocomposite based on methacrylic-Siloxane resin and surface-modified TiO2 nanocrystals, ACS Appl. Mater. Interfaces 7 (2015) 15494–15505.
[15] C. Esposito Corcione, A. Greco, A. Maffezzoli, Photopolymerization kinetics of an epoxy-based resin for stereolithography, J. Appl. Polym. Sci. 92 (2004) 3484–3491.
[16] L. Guo, S. Jiang, T. Qiu, et al., Miniemulsion polymerization of fluorinated siloxane-acrylate latex and the application as waterborne textile finishing agent, J. Appl. Polym. Sci. 131 (2014), n/a–n/a.
[17] H.M. Szczepanowska, Conservation of Cultural Heritage: Key Principles and Approaches, Routledge, 2013.
[18] A. Cataldi, A. Dorigato, F. Deflorian, A. Pegoretti, Thermo-mechanical properties of innovative microcrystalline cellulose filled composites for art protection and restoration, J. Mater. Sci. 49 (2014) 2035–2044.
[19] D. Burgentzlé, J. Duchet, J.F. Gérard, A. Jupin, B. Fillon, Solvent-based nanocomposite coatings: I. Dispersion of organophilic montmorillonite in organic solvents, J. Colloid Interface Sci. 278 (2004) 26–39.
[20] A. Licciulli, C. Esposito Corcione, A. Greco, V. Amicarelli, A. Maffezzoli, Laser stereolithography of ZrO2 toughened Al2O3, J. Eur. Ceram. Soc. 25 (2005) 1581–1589.
[21] A. Kiziltas, D.J. Gardner, Y. Han, H.S. Yang, Dynamic mechanical behavior and thermal properties of microcrystalline cellulose (MCC)-filled nylon 6 composites, Thermochim. Acta 519 (2011) 38–43.
[22] A.P. Mathew, K. Oksman, M.M. Sain, Mechanical properties of biodegradable composites from poly lactic acid (PLA) and microcrystalline cellulose (MCC), J. Appl. Polym. Sci. 97 (2005) 2014–2025.
[23] A. Cataldi, F. Deflorian, A. Pegoretti, Poly 2-ethyl-2-oxazoline/microcrystalline cellulose composites for cultural heritage conservation: mechanical characterization in dry and wet state and application as lining adhesives of canvas, Int. J. Adhes. Adhes. 62 (2015) 92–100.
[24] G.S. Springer, Environmental Effects on Composite Materials, Technomic Pub. Co., 1981.
[25] W.P. Paplham, R.A. Brown, I.M. Salin, J.C. Seferis, Absorption of water in polyimide resins and composites, J. Appl. Polym. Sci. 57 (1995) 133–137.
[26] Y.H. Cui, X.X. Wang, Q. Xu, Z.Z. Xia, Research on moisture absorption behavior of recycled polypropylene matrix wood plastic composites, J. Thermoplast. Compos. Mater. 24 (2010) 65–82.